# METEOSAT STUDIES OF CLOUDS AND RADIATION BUDGET

R. W. Saunders*
University College London
London, England

## INTRODUCTION

Three aspects of the work being carried out in the Laboratory for Planetary Atmospheres, University College London, are presented. Radiation budget studies of the atmosphere/surface system from Meteosat, cloud parameter determination from space, and sea surface temperature measurements from AVHRR data are all described. This work was carried out on the Interactive Planetary Image Processing System (IPIPS), which allows interactive manipulation of the image data in addition to the conventional computational tasks. The current hardware configuration of IPIPS is shown in figure 1. The $I^2S$ is the principal interactive display allowing interaction via a trackball, four buttons under program control, or a touch tablet. Simple image processing operations such as contrast enhancing, pseudocoloring, histogram equalization, multispectral combinations, etc. can all be executed literally at the push of a button. For the studies described here, Meteosat and NOAA AVHRR data were analyzed to give the results presented.

## RADIATION BUDGET STUDIES

Albedos and longwave fluxes are derived from the raw Meteosat images according to the scheme shown in figure 2. Having located the images so that each pixel can be assigned a latitude/longitude, the Meteosat visible images are converted into a map of broadband albedo using the calibration derived by Kriebel (1981). The calibration factor is a function of the underlying surface type because of the different frequency dependence of the reflected radiation (within the filter profile) from different surfaces. The calibration converts counts to radiances within the 0.4- to 1.1-μm region, and it is then assumed that the unfiltered albedo is the same as the filtered albedo within the above wavelength limits. The unfiltered albedo is given by:

$$a = \frac{\pi n_r}{sf \cos Z(t)} \qquad (1)$$

---

*Present affiliation: Rutherford Appleton Laboratory, Chilton, Didcot, Oxfordshire OX11 0QX, England.

where

$n_r$ filtered reflected radiance

s filtered solar constant

f Earth-Sun distance correction factor from 1 AU

Z(t) solar zenith angle at time t

The albedo derived is then corrected for anisotropic scattering effects by the following expression for each surface type m:

$$A_m = \frac{a_m(\theta,\phi,Z)}{X_m(\theta,\phi,Z)} \qquad (2)$$

where $X_m$ is the Nimbus 7 ERB anisotropic factor (Stowe et al., 1980) for model type m, viewing zenith angle $\theta$, relative azimuth angle $\phi$ (between Sun and satellite), and solar zenith angle Z.

The 11-μm IR channel was calibrated, according to Morgan (1980), who computed calibration factors from radiosonde and ship data. The conversion from filtered to broadband radiance was first carried out using a regression relationship developed by Abel and Gruber (1979), and more recently using a relation developed by Gube (1980). Limb darkening effects (Rashke et al., 1973) were also included. Good agreement was found between the results obtained from both regression relationships.

The albedos and longwave fluxes were determined over Western Europe, averaged over $1^{\circ}$ latitude/longitude squares for every hour of the day (21 August 1978). The instantaneous values at 1145 GMT are shown in figure 3, together with the original visible and infrared images from which these parameters were derived. The Meteosat data were obtained hourly so that the fluxes could be measured throughout 1 day. This allowed calculation of a true diurnal mean and the standard deviation of the values about the mean, as shown in figure 4. The regions of high visible standard deviations correspond to areas over which clouds formed and dissipated during the day. The diurnal heating of the cloud-free land surfaces also results in a higher standard deviation than that over the adjacent sea surfaces.

Diurnal variations are important when trying to infer an accurate daily mean from just one or two polar orbiter observations. Variations over different cloud and surface types have been measured (Saunders and Hunt, 1980) and are shown to be appreciable over cloud-free land (for outgoing flux) and over low stratocumulus clouds (for reflected flux). It is possible to model some of these variations for cloud-free scenes by looking at the Meteosat observations over many different surface types. These models can then be used to predict more accurate daily means from just one shortwave or two longwave polar orbiter observations.

Over cloud-free land or ocean the daily mean albedo $\bar{A}$ can be expressed as:

$$\bar{A} = \frac{1}{nSf} \frac{\sum_{i=1}^{n} Wr_i}{\sum_{i=1}^{n} \cos Z_i} \simeq \frac{Wr(\text{polar})}{Sf \cos Z(\text{polar})} \qquad (3)$$

where

$Wr_i$ reflected irradiance for the $i^{th}$ hour observed by Meteosat

n number of Meteosat observations for the day

S unfiltered solar constant

f Earth-Sun distance correction factor

$Z_i$ the solar zenith angle for the $i^{th}$ hour

Similarly, the mean outgoing flux $\bar{W}_E$ over cloud-free land can be expressed as:

$$\bar{W}_E = \frac{1}{n} \sum_{i=1}^{n} W_{Ei} \simeq \frac{W_{E,D}(\text{polar}) - W_{E,N}(\text{polar})}{\cos Z_D} \overline{\cos Z} + W_{E,N}(\text{polar}) \qquad (4)$$

where

$W_{E,D}(\text{polar})$, $W_{E,N}(\text{polar})$ daytime and nighttime polar orbiter observations of outgoing flux

$\overline{\cos Z}$ mean solar zenith angle for daylight hours

$Z_D$ solar zenith angle an hour before daytime polar orbiter measurements

Over cloud-free ocean, equation (4) can be simplified to:

$$\bar{W}_E = \frac{1}{n} \sum_{i=1}^{n} W_{Ei} \simeq \frac{W_{E,D}(\text{polar}) + W_{E,N}(\text{polar})}{2} \qquad (5)$$

Over clouds, both albedo and longwave flux are strongly dependent on cloud amount and height during the day. It is impossible to formulate a universal diurnal model for cloudiness, since different latitudes and seasons experience

different cycles of cloudiness. Over the tropics there is a predictable diurnal cycle for the cumulonimbus clouds over the land, and recent work by Minnis and Harrison (1981) and Gube (1980) has shown that many other types of clouds also have diurnal cycles. The difficulties arise at midlatitudes, where synoptic features which are not linked to the diurnal cycle dominate the changes in cloudiness. In this case more than two observations per day are necessary in order to get an accurate daily mean from polar orbiters. This is an important point when considering the merits of a one- or two-polar-orbiter observation system.

A recent study by Saunders et al. (1982) has compared Nimbus 7, Meteosat, and TIROS-N (Gruber and Winston, 1978) radiation budget measurements. Twelve target areas were chosen over the Meteosat field of view, each with differing cloud/surface types and temporal variations. The daily means from the three different satellite systems were compared, and the best agreement was found between the Nimbus 7 ERB longwave flux values and the corresponding Meteosat values, as shown in figure 5. Differences between the values are due to insufficient diurnal sampling from just two ERB observations, inaccurate narrowband-to-broadband algorithms for the Meteosat filter profile, and differences between the scenes viewed in the Meteosat and ERB target areas. The latter uncertainty was reduced as much as possible by choosing uniform target areas over which the emitted and reflected fluxes were not varying rapidly. Doubts about the narrowband-to-broadband radiance conversions were investigated by comparing coincident Meteosat and Nimbus 7 ERB radiances for approximately the same viewing angles. The total reflected radiances inferred from the Meteosat VIS channel agreed to within 10 percent of the measured ERB radiances, and the total emitted radiances inferred from Meteosat were within 2.5 percent of the ERB values.

## CLOUD STUDIES

Obtaining cloud parameters (amount and type) from satellite data is becoming increasingly important. The International Satellite Cloud Climatology Project (ISCCP) is now investigating the problems of obtaining a global cloud data set from the geostationary and polar orbiter data. Intercalibration of the satellites is one difficulty; this may be solved by using the polar orbiter, which underflies all of the geostationary satellites, to provide calibration data (Beriot et al., 1982). Gaps caused by missing geostationary satellites can also be filled at least once a day by the polar orbiter.

In order to obtain a global cloud climatology, the following parameters should be derived: total cloud amount over a predefined grid size (250 × 250 km for ISCCP), and amounts and heights of four well-defined classes, low, medium, convective, and cirrus clouds, measured once every 3 hours.

There are currently many different algorithms which can be used to extract cloud parameters from satellite radiance measurements. The threshold technique is the simplest, and with some refinements it can give accurate results. One problem with this method is that it assumes that the individual pixel either is completely filled with cloud or is cloud-free (Coakley and Bretherton, 1982). Also, gain changes in the radiometer must be accurately monitored in order to

give consistent results. One extension of the threshold technique is to use two wavelengths (VIS and IR). The advantages of this bispectral approach are that low cloud is more easily detected during the day from the VIS channel, and cirrus cloud is easily detected using the IR channel. With many days of measurements over each region, a minimum (cloud-free) albedo and maximum (clear) IR radiance can be determined for every region, so that varying thresholds are used according to the properties of the underlying surface type. For instance, clouds are easier to detect over a dark ocean surface than over bright deserts.

Other methods for extracting cloud parameters from satellite measurements include using sounder data to give cloud top heights and cloud amounts (Wielicki and Coakley, 1981), using stereo techniques from two satellites with different viewpoints of the same cloud (Hasler, 1981), and using bidimensional histograms to discriminate between different cloud types. Results from the threshold method and the bidimensional histogram method are presented here.

Cloud amounts over Europe are shown in figure 6 for 1145 GMT on 21 August 1978. In this case there were three classes defined, separated according to the cloud top temperature. These cloud amounts were derived with a threshold technique using both the VIS and IR channel information. Comparison with the associated visible image (fig. 6(a)) gives an idea of accuracy. Problems in using the threshold method are:

1. Low cloud at night; to overcome this the last daylight visible observation can be used as a constraint on the derived cloud amount from the IR channel

2. Areas of sunglint; only the IR channel should be used over these areas over ocean

3. Clouds over snow or ice; the 3.7-μm channel on AVHRR has proved a useful tool for discriminating between clouds and snow or ice surfaces

4. Low clouds over desert areas at night; this can be avoided by modeling the variation of IR radiance under cloud-free conditions during the night

5. Thin cirrus detection; the 6.3-μm water vapor (WV) channels on Meteosat and 3.7-μm on AVHRR can both detect thin cirrus more easily than the conventional VIS and IR channels

Another approach we have studied uses bidimensional histograms. Figure 7 compares such histograms over low and high cloud using all three Meteosat channels. The different positions of the histogram peaks demonstrate how different cloud types can be separated. The importance of using the IR-WV combination is that observations can be made at night, whereas the VIS-IR combination can obviously only be used in daylight.

## SEA SURFACE TEMPERATURE STUDIES

Methods have been developed for the analysis of sea surface temperatures (SST) from both TIROS-N and Meteosat images. In temperate latitudes, where the atmospheric water vapor absorption is relatively low, high-resolution (~1 km) sea surface temperature maps may be produced from cloud-free areas, as shown in figure 8(a) for the area around the UK on 12 July 1979. This map was obtained from TIROS-N AVHRR measurements, using data provided by ships to give a relative calibration (Saunders et al., 1982). The satellite-derived data provide considerably more structure in measurements of SST than can be derived from the corresponding ship measurements (fig. 8(b)).

An important feature in these data is the warm region of water to the north of the Netherlands. The center of this area was as much as 3.5°C warmer than the surrounding sea at 1500 GMT. The temporal variation of this feature was investigated using Mercator projected Meteosat images. To investigate the variation in a quantitative manner, a cross-calibration between the Meteosat and TIROS-N observations was developed.

From an analysis of the surface winds, it was found that the observed warm area appeared to be at the center of a ridge of high pressure where there was relatively low wind stress. Pingree and Griffiths (1978) have shown that this area is in a stratified regime during the summer months, which assists in inhibiting the mixing over a deep layer.

The energy balance of the ocean surface layer was modeled in order to simulate the temperature variation of the warm region (fig. 9). The best agreement with Meteosat data is obtained when a mixing layer of 0.6 m depth is assumed. This study eliminates the possible explanation that the anomaly was due to less atmospheric water vapor in this region. It was found that 8 mm of precipitable water would have to be removed from the atmospheric column through descent to achieve a temperature rise of 3.5 K. However, to achieve the observed heating rate, vertical velocities of 5 cm $s^{-1}$ are required, which would cause the radiance to stabilize after 12 hours. This is incompatible with the TIROS-N observation of a temperature anomaly at noon on the previous day, which is strongly suggestive of a diurnal variation.

This study demonstrates the importance of combining both polar orbiter and geostationary data in order to obtain good spatial, radiometric, and temporal resolution. This applies to studies of radiation budget, clouds, and sea surface temperature.

## REFERENCES


Abel, P. G.; and Gruber, A. 1979: An Improved Model for the Calculation of Longwave Flux at 11 μm. NOAA Tech. Memo. NESS 106.

Beriot, N.; Scott, N. A.; Chedin, A.; and Sitbon, P. 1982: Calibration of Geostationary Satellite Infrared Radiometers Using the TIROS-N Vertical Sounder. Application to Meteosat - 1. J. Appl. Met., vol. 21, no. 1, pp. 84-89.

Coakley, J. A., Jr.; and Bretherton, F. P. 1982: Cloud Cover From High Resolution Scanner Data: Detecting and Allowing for Partially Filled Fields of View. (Submitted to J. Geophys. Res.)

Gruber, A.; and Winston, J. S. 1978: Earth-Atmosphere Radiation Heating Based on NOAA Scanning Radiometer Measurements. Bull. Amer. Met. Soc., vol. 59, no. 12, pp. 1570-1573, Dec.

Gube, M. 1980: Outgoing Longwave Flux Computation From Meteosat Data. ESA Journal, vol. 4, no. 4, pp. 381-396.

Hasler, A. F. 1981: Stereographic Observations From Geosynchronous Satellites: An Important New Tool for the Atmospheric Sciences. Bull. Amer. Met. Soc., vol. 62, no. 2, pp. 194-212, Feb.

Kriebel, K. T. 1981: Calibration of the Meteosat VIS Channel by Airborne Measurements. Appl. Optics, vol. 20, no. 1, pp. 11-12, Jan.

Minnis, P.; and Harrison, E. F. 1981: Diurnal Variability of Regional Cloud Radiative Parameters From Geostationary Satellite Data. Paper presented at Fourth Conf. on Atmospheric Radiation, Toronto, June.

Morgan, J. 1980: Meteosat 1 Calibration Report, Issue 8, European Space Operational Center MDMD/MET.

Pingree, R. D.; and Griffiths, D. K. 1978: Tidal Fronts on the Shelf Seas Around the British Isles. J. Geophys. Res., vol. 83, no. C9, pp. 4615-4622, Sept. 20.

Rashke, E.; Vonder Haar, T. H.; Pasternak, M.; and Bandeen, W. R. 1973: The Radiation Balance of the Earth-Atmosphere System From Nimbus 3 Radiation Measurements. NASA TN-7249, p. 73.

Saunders, R. W.; and Hunt, G. E. 1980: Meteosat Observations of Diurnal Variation of Radiation Budget Parameters. Nature, vol. 283, no. 5748, pp. 645-647, Feb. 14.

Saunders, R. W.; Ward, N. R.; England, C. F.; and Hunt, G. E. 1982: Satellite Observations of Sea Surface Temperature Around the British Isles. Bull. Amer. Met. Soc. (To be published.)

Saunders, R. W.; Stowe, L. L.; and Hunt, G. E. 1982: An Intercomparison Between Radiation Budget Estimates From Meteosat 1, Nimbus 7, and TIROS-N Satellites. (Submitted to J. Appl. Met.)

Stowe, L. L.; Taylor, V. R.; Jacobowitz, H.; Ruff, I.; Chen, M.; Baldwin, E.; Van Cleef, F.; Hill, M.; and Coleman, D. 1980: A Unique Data Base for Studying Reflectance and Emittance Characteristics of Earth and Cloud Surfaces. Paper presented at International Radiation Symp., Fort Collins, Colorado, Aug.

Wielicki, B. A.; and Coakley, J. A., Jr. 1981: Cloud Retrieval Using Infrared Sounder Data: Error Analysis. J. Appl. Met., vol. 20, no. 2, pp. 157-169, Feb.

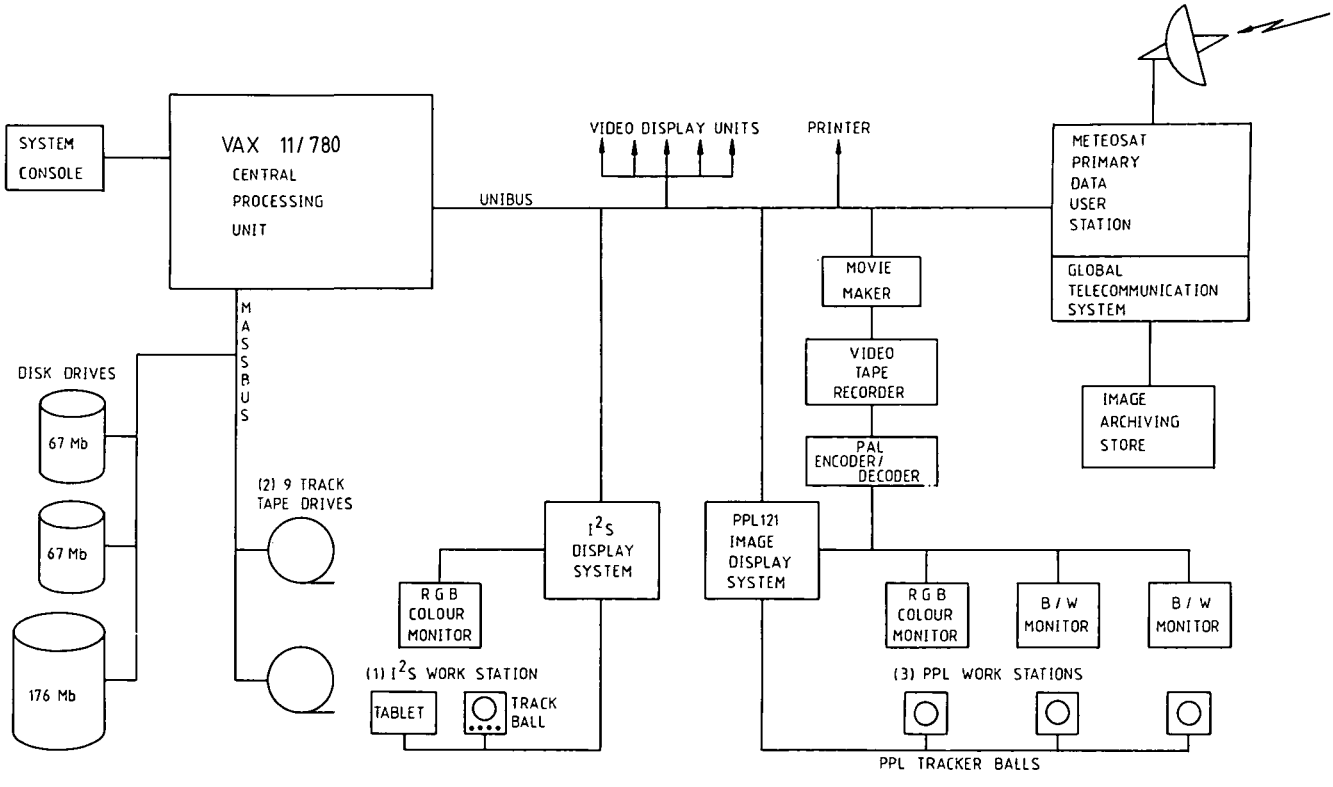


Figure 1.- Current hardware configuration of IPIPS.

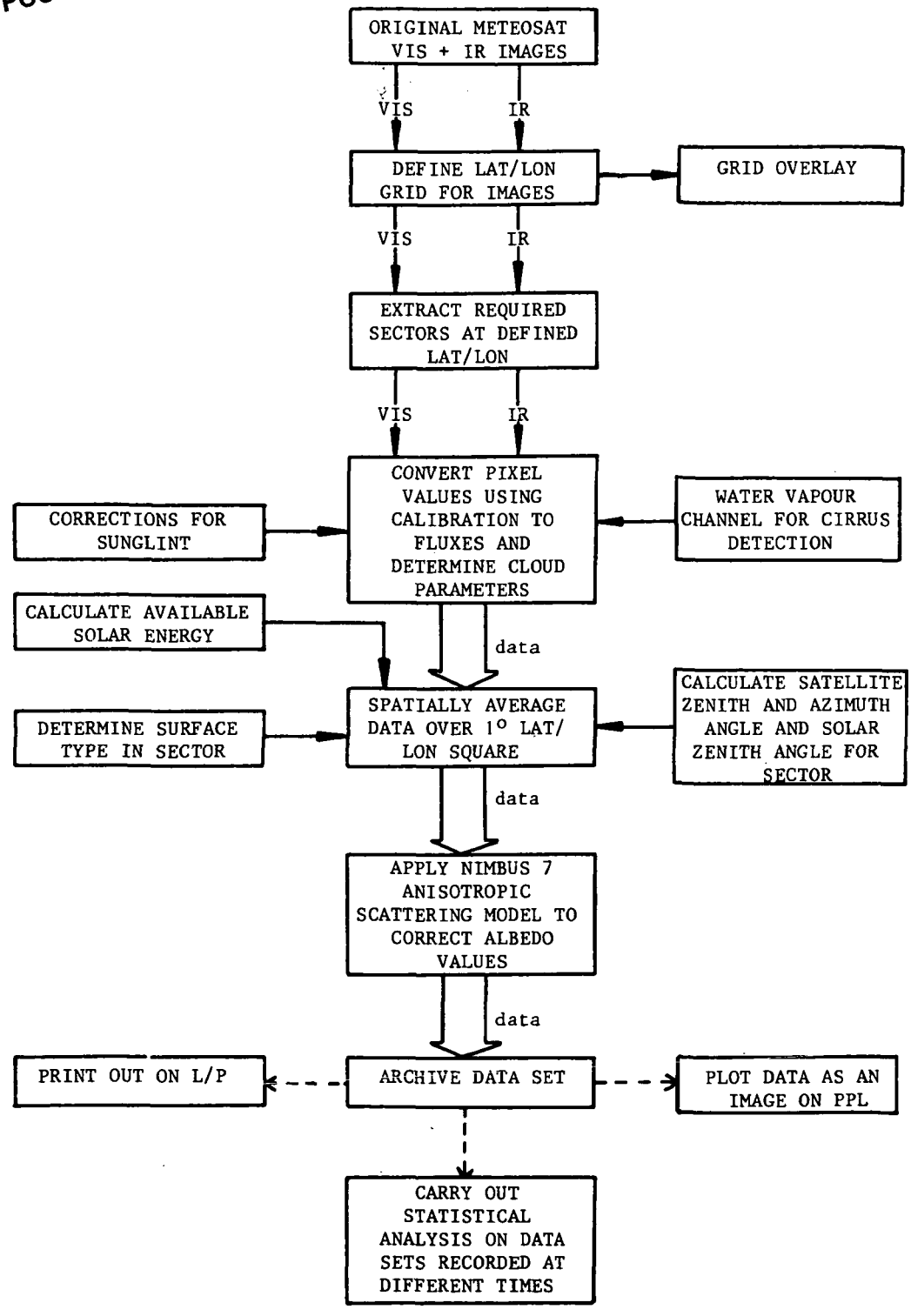


Figure 2.- Flow diagram for obtaining radiation budget parameters from raw image data.

(a) Visible.

(b) Infrared.

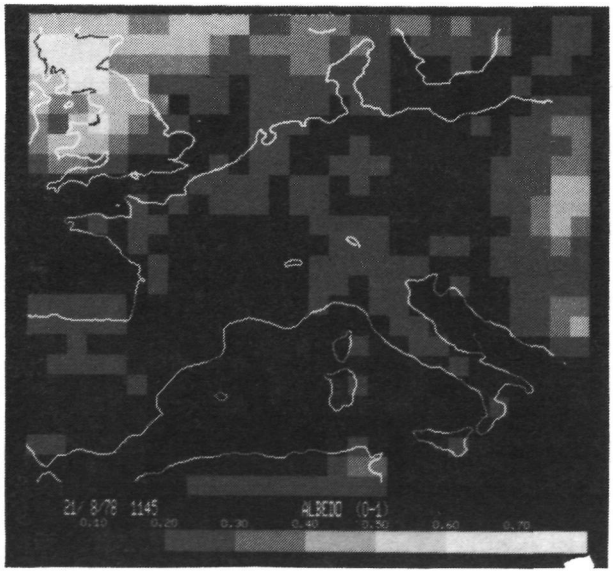


(c) Albedo.

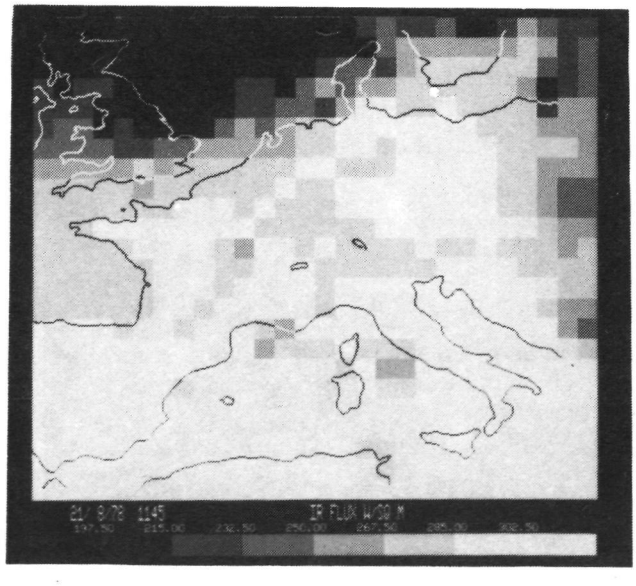


(d) Outgoing flux.

Figure 3.- Visible and infrared square projections of Europe from Meteosat and the albedo and outgoing flux averaged over $1^{o}$ latitude/longitude squares, derived from the VIS and IR satellite images for 1145 GMT on 21 August 1978. The parameter values are displayed according to the greyscale along the bottom.

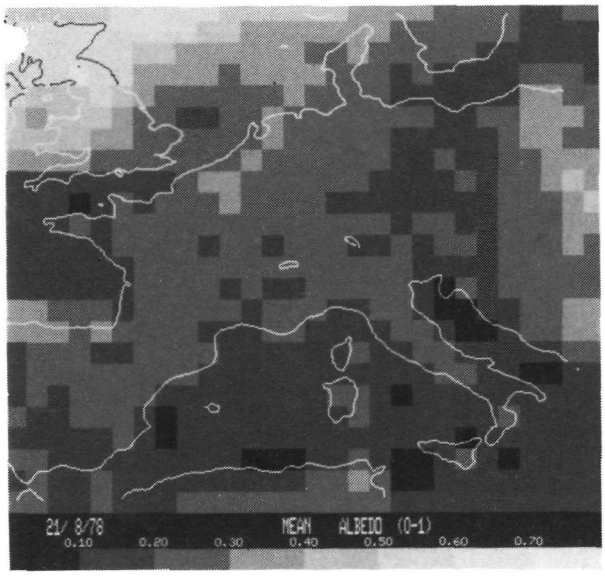


(a) Mean albebo.

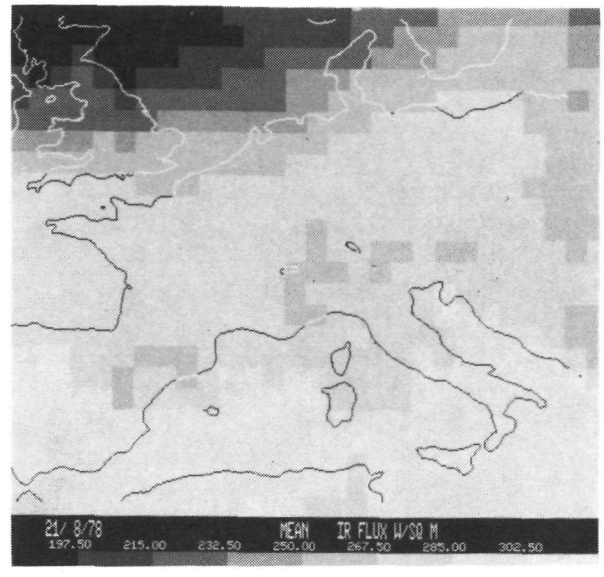


(b) Mean longwave flux ($W/m^2$).

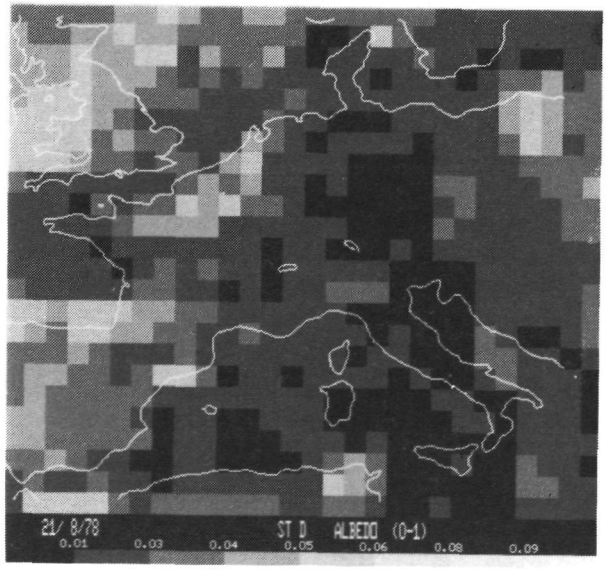


(c) Standard deviation of albedo.

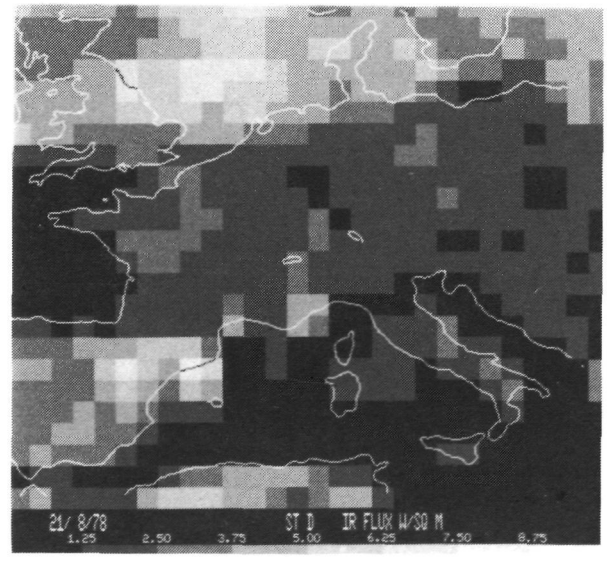


(d) Standard deviation of longwave flux ($W/m^2$).

Figure 4.- Mean albedo, longwave flux, and their standard deviations for 21 August 1978 over Europe. The values are displayed according to the greyscale.

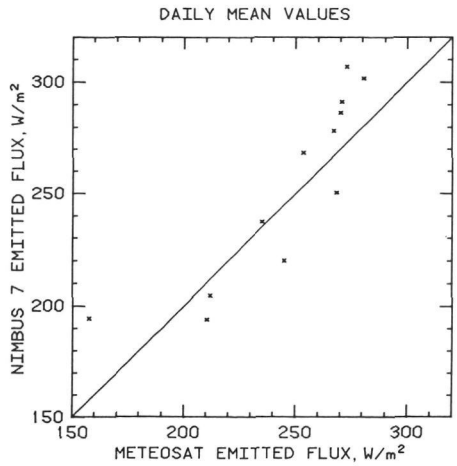


Figure 5.- Comparison of Nimbus 7 ERB and Meteosat daily mean emitted fluxes over 12 uniform target areas for 14 October 1979.

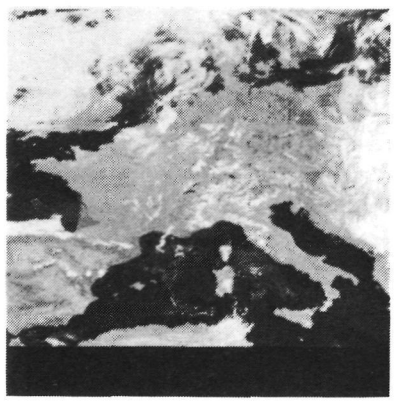

(a) Visible Meteosat square projection.

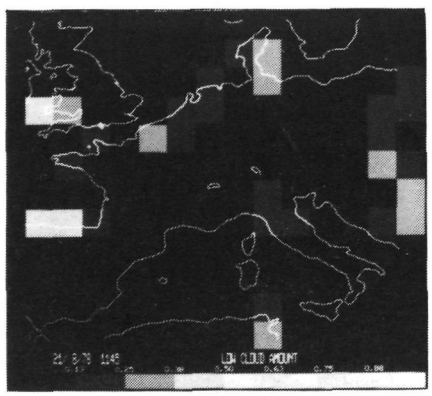

(b) Low-cloud amounts.

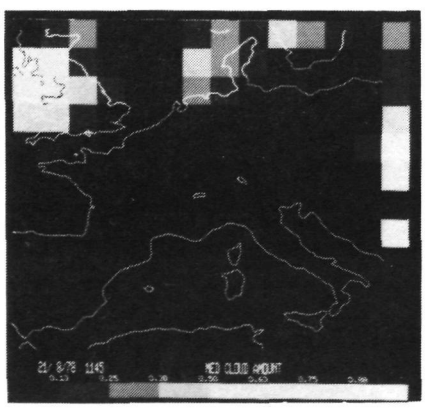

(c) Medium-cloud amounts.

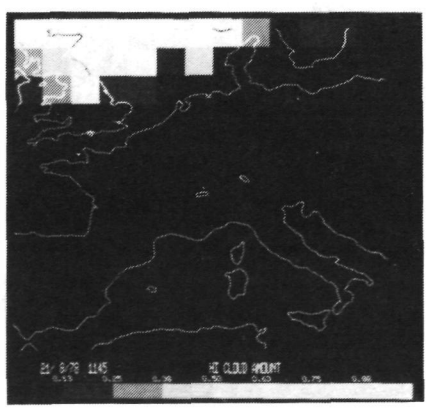

(d) High-cloud amounts.

Figure 6.- Visible Meteosat square projection and low-cloud, medium-cloud, and high-cloud amounts averaged over $2^{o}$ latitude/longitude squares derived from the VIS and IR satellite images for 1145 GMT on 21 August 1978. The minimum-cloud amount shown on this plot is 10 percent. The actual data record cloud amounts down to 1 percent.

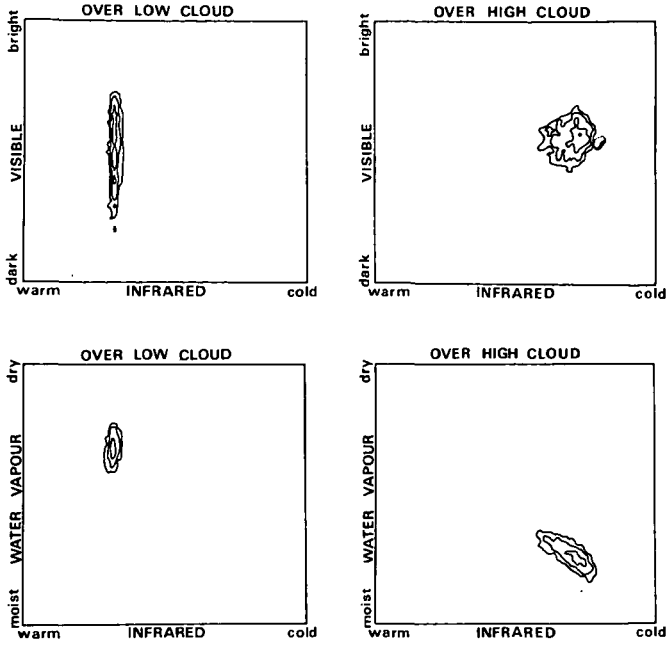


Figure 7.- Examples of bidimensional histograms over low and high clouds from Meteosat. Both VIS-IR and IR-WV combinations are shown.

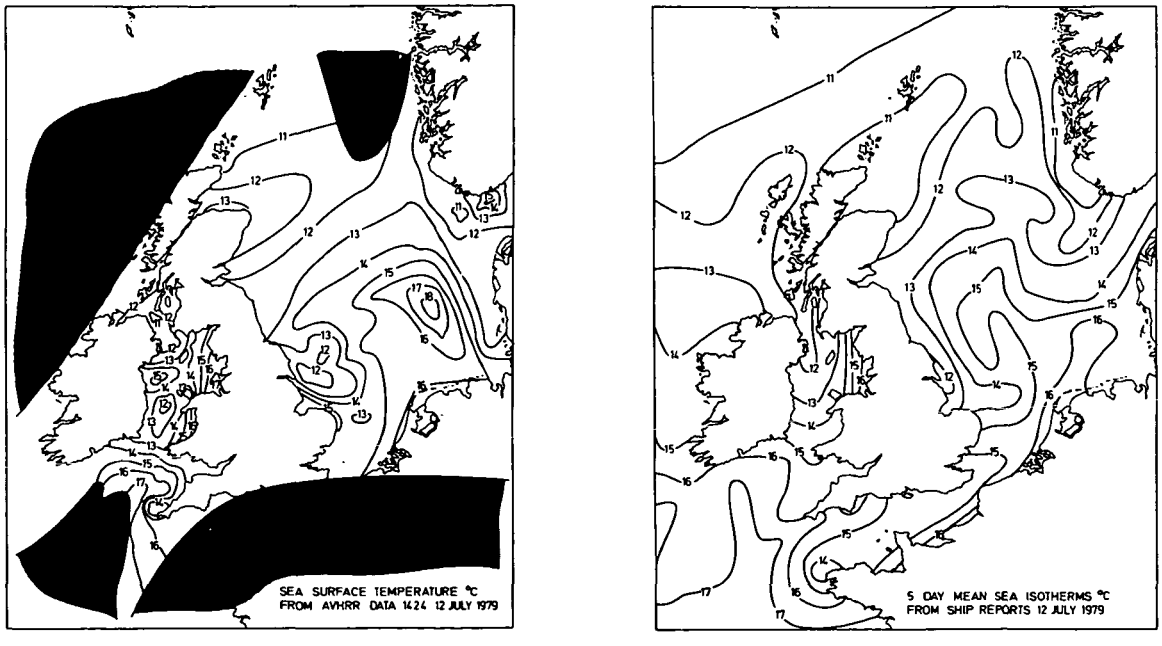


(a) (b)

Figure 8.- Isotherms of sea surface temperatures around the British Isles for 12 July 1979 from AVHRR 11-μm data, 1424 GMT (a), and ship reports, 1200 GMT (b).

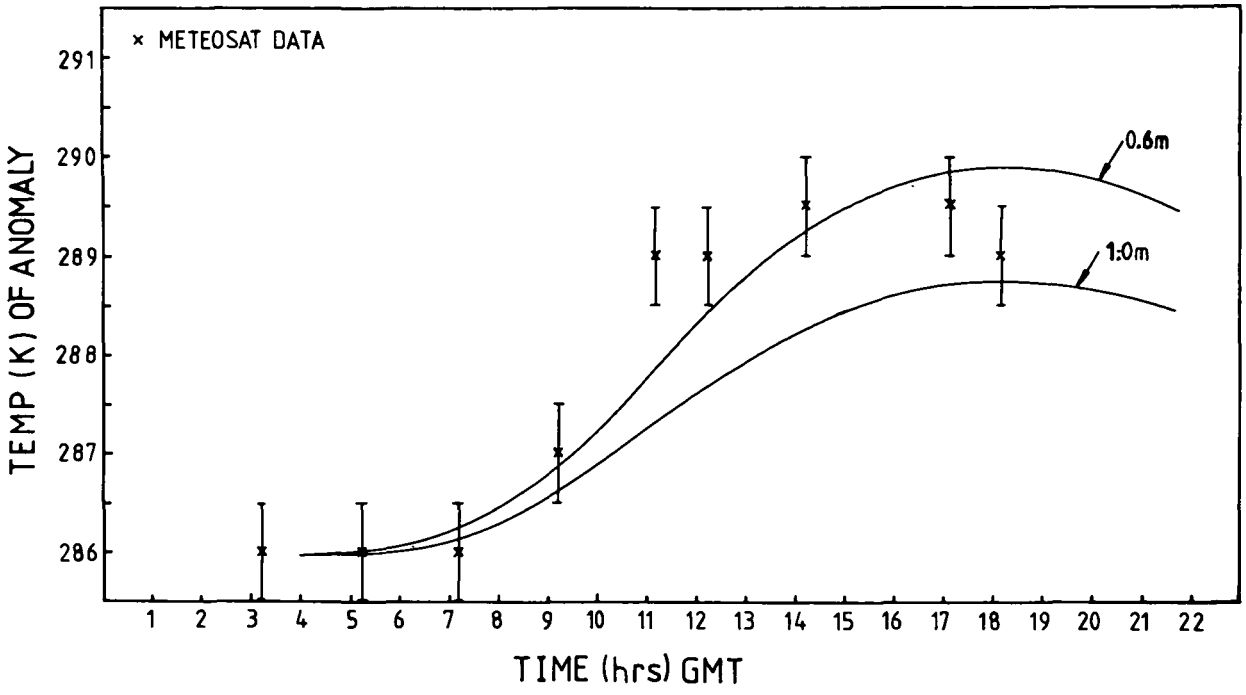


Figure 9.- Variation of sea surface temperature at the center of the anomaly as a function of time. The crosses denote Meteosat measurements. The solid lines represent predictions from a simple one-dimensional heat transfer model for different assumed mixing depths.